

Chapter 2

Development of Physics-Based Modeling for ULSI Interconnections Failure Mechanisms: Electromigration and Stress-Induced Voiding

As mentioned in [Chap. 1](#), the two major failure mechanisms in ULSI interconnections are electromigration and stress-induced voiding. In this chapter, we will provide reviews on the model development for electromigration and stress-induced voiding.

2.1 Electromigration (EM) Modeling Review

In this chapter, we present a comprehensive review on the physics-based modeling of EM phenomena in ULSI interconnections over the last three decades. In the evolution of the physics-based modeling, some aspects of the physics are dropped for simplification, and some are added to accommodate new understanding on the EM physics as well as for the new development of the interconnect technology. With the continuous change in the metallization system and materials, the aspects of physics that have been dropped may become important again, and new physics might also occur with these changes in metallization system. Here, we re-examine the justification of dropping or adding various physical aspects in the EM modeling during their evolution and their implications on the future interconnect system.

2.1.1 One-Dimensional (1D) Analytical Modeling

Like most physical modeling, physics-based EM modeling began from 1D analytical modeling by solving the following continuity equation [1] derived from the time evolution of the vacancy concentration along an interconnect line:

$$\frac{\partial C_v}{\partial t} + \frac{\partial J_v}{\partial x} + r = 0. \quad (2.1)$$

Here C_v is the instantaneous vacancy concentration at position x and time t , J_v is the vacancy flux due to EM-driving forces and r is the sink/source term which allows for the recombination or generation of vacancies at sites such as grain boundary, dislocations, or surface [1].

The focus of this 1D modeling is on the simulation of EM kinetics. The net vacancy flux along the length of an interconnect can be due to the electron wind force, vacancy diffusion as a result of concentration gradient (Fickian diffusion) and temperature gradient (Soret diffusion), hence the flux can be written as [1]

$$J_v = -D \frac{\partial C_v}{\partial x} + \frac{DC_v Z^* e E}{k_B T} + \frac{Q^* DC_v}{k_B T^2} \cdot \frac{\partial T}{\partial x} \quad (2.2)$$

where D is the vacancy diffusivity given by $D = D_0 \exp(-\Delta E_a / k_B T)$, E_a is the activation energy for the vacancy diffusion, $Z^* e$ is the effective charge of the diffusing species, E is the electric field and Q^* is the heat of transport.

The sink/source term r can be expressed as [1]

$$r = \frac{C_v - C_{ve}}{\tau} \quad (2.3)$$

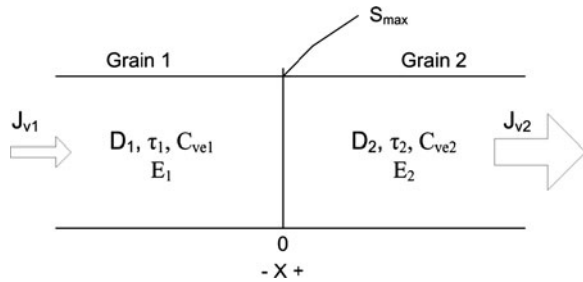
where C_{ve} is the equilibrium concentration of vacancies within a grain, and τ is the average lifetime of a vacancy.

Equation 2.1 is a basic EM equation from the first principle, and it was adopted by many 1D analytic EM models reported in the literature as will be discussed below. Various EM models were proposed based on different boundary conditions, and the phenomenon of EM were simulated by analyzing the evolution of the vacancy concentration in an interconnect metal line using Eqs. 2.1–2.3. In general, two categories were being considered in this 1D analytical modeling as follows.

2.1.1.1 Category #1: 1D Modeling Without the Consideration of Stress Gradient-Induced Migration

In one of the pioneer works on 1D continuum EM modeling, the work of Rosenberg and Ohring [2], the electron wind force, concentration gradients (Fickian diffusion), and temperature gradients are taken into consideration with the presence of the vacancy sink/source. As shown in Fig. 2.1, they proposed a model from the appropriate solution of Eq. 2.1 where it was assumed that two grains intersect at $x = 0$ and that each grain can be characterized by their respective vacancy diffusion parameters, namely the diffusivity D and the equilibrium vacancy concentration C_{ve} , the lifetime of the vacancy τ , and field strength E . The vacancy behavior as

Fig. 2.1 Model of two grain boundaries intersecting at $x = 0$. Reprinted with permission from Rosenberg and Ohring [2], copyright © 1971, American Institute of Physics



expressed by Eq. 2.1 was written separately for the two grains, assuming the diffusion parameters are constant within each grain.

In order for vacancy buildup to take place, it is necessary that the vacancy flux induced by the electron flow is different in the two grain regions. The boundary conditions used by Rosenberg and Ohring [2] were that the vacancy concentration and flux at $x = 0$ are continuous, and all the diffusion parameters are the same in the two grains except that the activation energies for diffusion are 0.6 eV for $x > 0$ and 0.8 eV for $x < 0$. Using Laplace transform method, both transient time-dependent solution and steady-state solution of $C_v(t)$ were obtained. The impact of temperature on EM kinetics and the discontinuity in grain size which causes an abrupt change in the number of atomic diffusion paths on the EM performance of a metal thin film were studied in their steady-state solution.

Their model simulated the vacancy saturation due to the divergence of vacancy flux at the grain boundary with the consideration of multiple EM-driving forces. Although the temperature gradient-induced migration was taken into consideration during their initial modeling of EM, it was dropped for the sake of simplicity during the actual calculation. For the justification of the simplification, they stated that the interconnect length was the only dimension considered in their 1D EM model, and the current density was evenly distributed throughout the length; thus the temperature along the length should be a constant as metals are very good heat conductor. However, in actual interconnection in today's ULSI, the effect of the temperature gradient can no longer be ignored as revealed by 3D modeling which will be discussed in Chap. 4. Also, the choice of the boundary condition with infinite ends in their model renders the model incapable of catering the length effect of a confined metal thin film; which was discovered by Blech few years later [3, 4]. Due to this incapability, this type of boundary condition was not chosen for subsequent 1D continuum EM modeling.

A more realistic boundary condition was proposed by Shatzkes and Lloyd [5]. In their study, the case of vacancy flow in the region of a purely blocking boundary was examined as shown in Fig. 2.2.

This condition can occur in real conductors, for instance, at the boundary of a "bamboo" grain. Mathematically, the boundary conditions for their case can be expressed as

$$C(-\infty, t) = C_0 \quad (2.4)$$

Fig. 2.2 Schematic drawing of the semi-infinite grain boundary considered in the work of Shatzkes and Lloyd [5]

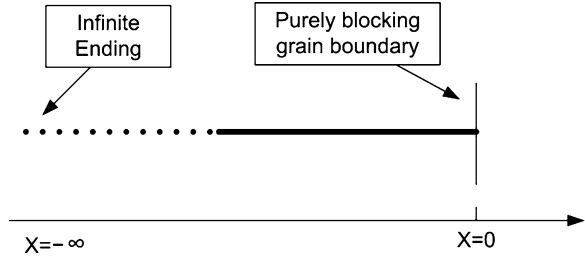
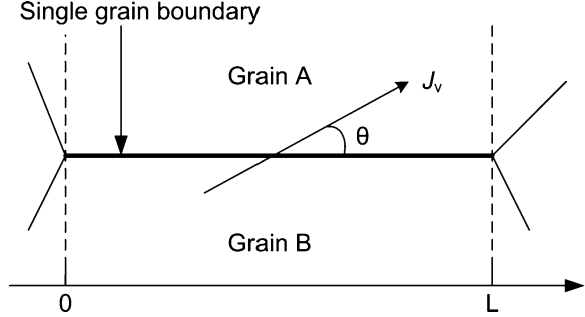


Fig. 2.3 Grain boundary between two triple points at $x = 0$ and $x = l$. The angle between the grain boundary and the current density j is labeled as θ . Reprinted with permission from Kirchheim and kaeber [6], copyright © 1991, American Institute of Physics



$$J_v(0, t) = 0. \quad (2.5)$$

Although this solution treats a special case of a perfectly blocking boundary, it is useful for the understanding of the boundary conditions that allow a reduced vacancy flow as pointed out by them. In general, there is a flux through any given region, but a divergence may still exist. By treating this “residual” mass flux as a background, we can then treat the accumulation of vacancies above the background in the present manner. In their study, assuming isothermal condition with no thermal transport, the vacancy flux due to temperature gradient-induced migration was not considered as well. The vacancy sink/source term was also dropped in their EM equation because the formation and annihilation of vacancies in the grains can become significant only at elevated temperature [6].

Based on the same EM equation, Kirchheim and Kaeber [6] reported their EM modeling and solved the EM equation based on different boundary conditions. They considered the case of a single grain boundary structure as shown in Fig. 2.3.

Compared with the infinite boundary condition proposed by Rosenberg and Ohring [2] and the semi-infinite boundary condition proposed by Shatzkes and Lloyd [5], Fig. 2.3 shows a special case of finite boundary that the fluxes at both ends are zero (i.e., due to very low vacancy mobilities in the adjacent grain boundaries), that is,

$$J_v(x = 0) = J_v(x = l) = 0. \quad (2.6)$$

In the work of Kirchheim and Kaeber, both the solutions with and without the consideration of vacancy sink/source were analyzed and discussed. Since the

formation and annihilation of vacancies in the grains occur only at elevated temperatures as mentioned earlier, they focused on the steady-state concentration profile without vacancy sinks/sources. In the calculation of vacancy flux, the grain boundary component of the electric field or current density was considered, i.e., the total current density was multiplied by $\cos \theta$ (refer to Fig. 2.3).

With this finite boundary condition, they simulated the mass backflow during EM. However, contrary to the generally accepted interpretation, where the mass backflow was a flow of matter caused by a stress gradient within the Al line [3, 4], their interpretation of the backflow was based on the diffusional backflow of vacancies with respect to the vacancy concentration profile. They argued that the vacancy fluxes and internal stress gradients are coupled since production and annihilation of vacancies is often accompanied by plastic deformation.

A more completed study on the boundary conditions of the EM equation was reported by Clement and Lloyd [7]. Similar to the previous studies, both the electron wind force and vacancy concentration gradient are taken into the consideration as driving forces of EM. In their report, the physical meanings of the three boundary conditions used were described and the solutions were compared at the blocking barrier. The first boundary condition corresponds to a situation of a semi-infinite metal line which is the same as the one proposed by Shatzkes and Lloyd [5]. The other two boundary conditions are for the cases of the finite interconnect length. The first case corresponds to a situation where the number of vacancies is conserved. An example of such case is an interconnect line with a thick and strong passivation layer that precludes volume change of the conductor, and such boundary condition and its corresponding solution have been reported by Kirchheim and Kaeber [6]. The second case corresponds to a situation where the passivation or adherent oxide layer on the metal line is not so strong and stiff as to preclude the creation of vacancies. This is what one might expect in an Al conductor covered only by its native oxide (Refer to Fig. 2.3). This new boundary condition can be expressed as:

$$J_v(L, t) = 0 \quad (2.7)$$

$$C(0, t) = C_0. \quad (2.8)$$

Solutions to the above-mentioned three reasonable boundary conditions for the EM equation were investigated numerically. It was shown that regardless of the boundary condition chosen, the time to failure would approximate the semi-infinite solution of Shatzkes and Lloyd as long as the critical failure vacancy concentration is significantly different from the vacancy concentration at equilibrium.

A complete review on the 1D EM modeling was contributed by Clement in his review paper [1]. He reviewed all the 1D EM models before 2001 from the perspectives of the consideration of driving forces of EM, choices of the boundary conditions, and the corresponding numerical solutions. In his report, the 1D EM models with the consideration of vacancy sink/source were compared to those without it. Although the numerical solutions of the EM equation for both cases are quite similar, there is one critical difference. The effect of the consideration of

vacancy sink/source is the shift in time scale for the buildup of vacancies. Hence, the calculated time-to-failure will be in the order of several days, rather than a few seconds, as obtained from those models without the consideration. This highlights the importance of including the sink/source term in the 1D EM model. In his report, he also discussed the importance of critical components in 1D EM model, such as critical stress to initiate the void formation or dielectric cracking, critical void size to cause the failure of the interconnect, and current density dependence near the critical stress and void size. However, the aforementioned 1D EM overlooks the importance of stress effect during EM. Different hypothesis on the effect of stress during EM were proposed in the literature, and it was clear that the ignorance of stress effect in EM modeling would render inaccuracy in the prediction.

2.1.1.2 Category #2: 1D Modeling with the Consideration of Stress Gradient-Induced Migration due to Back Stress

With the shrinking interconnect line dimensions, it is found that, in the confined metal interconnects deposited on an oxidized silicon substrate and covered by a dielectric passivation layer, EM gives rise to back stresses that can retard EM itself [8]. A few reports on the modeling of EM incorporating the effect of the transient back stress buildup can be found, such as Ross [9], Kirchheim [10], and Korhonen et al. [11]. The modeling of the EM-driving forces was modified to account for the effect of the migration due to stress gradient.

For example, in the work by Kirchheim [10], additional EM-driving force, the stress gradient, was taken into consideration. Moving an atom from the grain boundaries to the surface changes the volume by one atomic volume, Ω . Allowing relaxation of the neighboring atoms leads to a contraction in volume of $f\Omega$ ($0 < f < 1$), and hence the total volume change is $(1 - f)\Omega = f'\Omega$. With the presence of this strain, a stress gradient is produced, and the corresponding vacancy flux is given by

$$J_{\sigma} = -\frac{DC_v}{kT}f\Omega\frac{\partial\sigma}{\partial x}. \quad (2.9)$$

With this additional driving force, Eq. 2.2 was modified as

$$J_v = -D\frac{\partial C_v}{\partial x} + \frac{DC_v Z^* e E}{k_B T} + \frac{Q^* DC_v}{k_B T^2} \cdot \frac{\partial T}{\partial x} - \frac{DC_v}{kT} f\Omega \frac{\partial\sigma}{\partial x} \quad (2.10)$$

In their modeling, the atomic migration due to the temperature gradient was also neglected with the same argument as given by Rosenberg and Ohring [2]. Vacancy sink/source was considered in a similar way as in Eq. 2.3. The generation of a vacancy changes the volume by $\Delta V/V = f'\Omega$ and, therefore, the rate of the volume change within a grain of diameter d is related to the rate of vacancy generation within the grain boundary of thickness δ by

$$\frac{1}{V} \frac{\partial V}{\partial t} = f' \Omega \frac{\delta}{d} \frac{\partial C_v}{\partial t} = f' \Omega \frac{\delta}{d} \frac{C_v - C_{ve}}{\tau}. \quad (2.11)$$

Using the Hooke's Law which states that $\delta\sigma = B\delta V/V$, we have

$$\frac{\partial \sigma}{\partial t} = B f' \Omega \frac{\delta}{d} \frac{C_v - C_{ve}}{\tau} \quad (2.12)$$

where B is the bulk modulus of the metal line.

With the two coupled differential equations (2.10) and (2.12), the continuity equation (2.1) for the vacancy concentration and the rate equation (2.3) for the vacancies sink and source reactions, the EM phenomenon was simulated in a finite line blocked at both ends [$J_v(x=0) = J_v(x=l) = 0$] as shown in Fig. 2.3. The incorporation of mechanical stresses developing as a consequence of electromigration and vacancy annihilation and generation, leads to a complicated relationship between vacancy concentration and mechanical stress which can only be solved analytically for a few limiting cases. By coupling stress development with the vacancy concentration change along the metal line, the stress gradient can be calculated and the back flow due to the stress gradient can be simulated.

In the model developed by Korhonen et al. [11], the driving forces of EM included only the electron wind force and the stress gradient, and both driving forces were formulated based on the atomic flux instead of the vacancy flux. However, the vacancy sink/source term was dropped in their consideration because they assumed that the net number of atoms entering a volume element was large enough to include vacancy sources and sinks. In their modeling, the change in atomic concentration was also coupled with the stress evolution in a similar manner as in the work by Kirchheim [10], and they presented several representative cases, such as the semi-infinite metal line where the flux is blocked at the end $x=0$, and the confined finite metal line where the flux is blocked at both the ends. Besides the investigation of the EM equations with different boundary conditions, Korhonen et al. also studied the influence of the stress evolution on the diffusivity of atoms and its impact on the solutions to the EM equation. They derived the vacancy concentration as follows.

$$C_v = C_{v0} \exp(W_f + \Omega\sigma/kT) \quad (2.13)$$

where Ω is the atomic volume, W_f is the interaction energy between the vacancy and the stress field, and C_{v0} is the vacancy concentration in the absence of any stress effect. Additionally, the dependence of the vacancy diffusivity on the hydrostatic pressure p was also derived and included as follows.

$$D_v = D_v(0) \exp(-pV_m/kT) \quad (2.14)$$

where V_m is the dilatation associated with vacancy migration and $D_v(0)$ is the vacancy diffusion coefficient at $p=0$.

The constant diffusivity used in the early solution (Kirchheim) was actually in the absence of any stress effects. The numerical integration of stress-dependent

diffusivity in the EM model was accomplished by the method of finite differences. Surprisingly, numerical results with a stress-dependent diffusivity for the semi-infinite line turned out to be reasonably close to the analytic estimates with a constant diffusivity. Korhonen stated that the analytic solutions may in several cases be well sufficient for practical estimation of stress buildup during EM. However, for modeling of more complicated line structures, one must resort to numerical solution.

Although the EM equation formulated by Korhonen et al. [11] as discussed above is very similar to those by Rosenberg and Ohring [2], Shatzkes and Lloyd [5], Kirchheim and Kaeber [6], and Clement and Lloyd [7], the use of atomic flux with the consideration of the stress evolution by Korhonen et al. presented a retardation of EM damage due to the back stress. Such phenomena is not possible with vacancy flux approach as vacancy concentration gradient does not retard EM damage. Furthermore, significant vacancy concentration gradients can be created in a matter of seconds because of the almost negligibly small material transport involved. However, the stress evolution in the interconnect lines during EM can last hundreds of hours as predicted by Korhonen et al. [11] using the atomic flux approach.

With the development of the analytical modeling and interconnect technology, Korhonen's model received further review and continuous development in order to explain the physics of EM in advanced interconnect systems. Clement and Thompson [12] reported a complete review on the Korhonen's model and found that the analytic solution for a semi-infinite line with a blocking boundary given by Korhonen et al. was a good approximation only when the stress buildup is small, and this is usually not the case for narrow, encapsulated interconnect lines in which the EM-induced stress can be very high prior to failure. They proposed a complete model description and a more accurate analytic solution to the differential equations describing the EM-induced stress buildup at a blocking boundary [12].

Based on their improved model [12], Park et al. reported another EM model to simulate the reliability of Al and Al-Cu interconnects [13]. In their work, the effect of the impurity Cu atoms in Al interconnects on stress evolution and lifetime was investigated in various structures. In addition, the significance of the effect of the mechanical stress on the diffusivity of both the Al and Cu was determined. Current density exponents of both $n = 2$ for void nucleation and $n = 1$ for void growth failure modes were found in both pure Al and Al-Cu lines. More importantly, the application of the model was further extended to the investigation of other interconnection materials such as Cu and its alloys by modifying the input material properties. The detailed mathematical formulation used in the analysis can be found in their report and earlier study [14]. Their analytic EM model was developed into an EM simulation package called MIT/EmSim [15] which was extensively employed in their other EM studies [16–18] and successfully provided theoretical support to various experimental observations.

Although the stress gradient-induced migration due to back stress has been well addressed by the models discussed above, another important source of the stress is overlooked in their theoretical consideration, and it is the thermo-mechanical stress due to the thermal mismatch between the metal line and its surrounding materials.

The thermo-mechanical stress depends on the thermal expansion coefficients of the materials and the shape of the metal line itself; and 1D EM models are incapable of simulating the effect.

2.1.2 Two-Dimensional (2D) Modeling

Besides the electron wind force, vacancy concentration gradient, stress, and temperature gradients, the EM performance of an interconnect is found to be greatly affected by the microstructural inhomogeneities of the line, such as the grain size and texture distributions, the triple points of the grain boundaries, the barrier layer interface, and the surrounding materials of the metal line [19]. While the EM equation is generally easy to solve in one dimension, the simplifications fail to account for the details of the effect of microstructures. A step further into the reality is achieved by using 2D models with the consideration of the microstructure of the metal conductor. The addition of this second dimension complicates the governing EM equations significantly, and numerical approaches are generally required to find the solution. Most of 2D EM models use the atomic flux to study the EM instead of using vacancy flux. Some of them focus on the atoms transport along different diffusion paths, under various EM-driving forces as well as the void nucleation and growth, while some of them focus on the void shape evolution due to the atom transport along the void surface. Let us consider their respective models.

2.1.2.1 2D EM Driving Force and Diffusion Path Model

In 1999, Gleixner and Nix reported their study on the simulation of EM [20]. In their study, both the thermo-mechanical stress and electron wind force were taken into consideration. They proposed a new method of solution for the coupled stress-diffusion equations in a 2D model while avoiding the computational complexity associated with the finite element approaches. The atomic flux which results from electron wind force and stress gradients were expressed in Eqs. 2.15 and 2.16 respectively, as follows,

$$J_a = \frac{D}{\Omega kT} Z^* e \rho j \quad (2.15)$$

$$J_a = \frac{D}{kT} \nabla \sigma \quad (2.16)$$

where J_a is the atomic flux and $\nabla \sigma$ is the stress gradient. The stress is due to both the Blech effect σ_n and thermo-mechanical stress σ_h . The total atomic flux is then given by the sum of both equations as follows.

$$J_a = \frac{D}{kT} \left(\nabla \sigma + \frac{Z^* e \rho j}{\Omega} \right). \quad (2.17)$$

In their 2D model, they treated the mass transport along the grain boundary; along the sidewall interfaces and inside the grain differently.

For the case of atoms transport along the grain boundary, the atomic flux was given as:

$$J_a = \frac{D_{gb}}{kT} \left(\frac{\partial \sigma_n}{\partial l} + \frac{Z^* e \rho j \cdot \cos \theta}{\Omega} \right) \quad (2.18)$$

where D_{gb} is the diffusivity along the grain boundary, l is the distance along the grain boundary, and θ is the angle between current flow and the grain boundary.

For the case of atoms transport along the sidewall, the flux was given as:

$$J_a = \frac{D_{ini}}{kT} \left(\nabla \sigma_n + \frac{Z^* e \rho j}{\Omega} \right) \quad (2.19)$$

where D_{ini} is the diffusivity along the interface between the sidewall and the metal thin film.

For the case of atoms transport inside the grain, the flux was given as:

$$J_a = \frac{D_b}{kT} \left(\nabla \sigma_h + \frac{Z^* e \rho j}{\Omega} \right) \quad (2.20)$$

where D_b is the diffusivity inside the grain. The diffusion through the bulk is driven by a hydrostatic stress gradient instead of the normal traction due to the Blech effect. The stress field solution was calculated before the start of the simulation.

The stress field solution obtained was superimposed along all the diffusion paths to find the total stress field in the material. The local stress gradient and the diffusivities were then coupled in the calculation of local atomic flux. In this way, the method avoided the computational complexity associated with finite element approaches, and they claimed that this approach was able to simulate stress evolution in complex microstructures very quickly and can therefore be applied to interconnect with realistic grain structures.

Another 2D EM model based on Cu interconnections was proposed by Sukharev and Zschech [21]. Instead of analyzing the vacancy flux in the EM Eq. 2.1, a mass balance equation for atomic concentration was adopted in their model as follows.

$$\frac{\partial N}{\partial t} + \nabla J = 0 \quad (2.21)$$

where $N(r, t) = N/N_0 = \Omega N$ is the normalized atomic concentration at the $r = (x, y, z)$ location at the moment of time t , $\Omega = 1/N_0$ is the atomic volume with N_0

as the initial atomic concentration, and J is the total atomic flux at this location. In their study, various driving forces were incorporated into the mass balance equation, such as the concentration gradients, the electron wind force, temperature gradients, and the mechanical stress gradient as follows.

Atomic flux due to concentration gradients was given as

$$J_N = -D\nabla N \quad (2.22)$$

Atomic flux due to electron wind force was given as

$$J_C = \frac{NeZ^*D\rho_j}{kT} \quad (2.23)$$

Atomic flux due to temperature gradient was given as

$$J_T = -\frac{NDQ}{kT^2}\nabla T \quad (2.24)$$

Atomic flux due to mechanical stress gradient was given as

$$J_s = \frac{ND\Omega}{kT}\nabla\sigma_h \quad (2.25)$$

Combining Eq. 2.21 and Eqs. 2.22–2.25, the atomic concentration at any point of the considered segment can be characterized for a given current density, temperature and stress gradients. In order to get a complete solution of the model, they determined the evolution of the current, temperature, and stress distributions in the considered segment. Similar to the model developed by Gleixner and Nix [20], different diffusivity values were introduced to simulate the effect of microstructure and surrounding material on atomic flux based on the process technology. The diffusivities along different interfaces, grain boundaries, and inside the bulk were treated differently to simulate the changes in the failure mechanism due to different process technologies. The predicted locations of the void nucleation sites as well as the predicted void dynamics in a variety of interconnect segments fitted well to the available experimental data [22, 23].

2.1.2.2 2D Void Surface Evolution Model

The simulation methodology for this class of model was initiated in the mid-1990s, and two different modeling methodologies were developed. Both of them are 2D models based on finite element analysis to calculate the governing equation for current density, temperature, and stress distributions in a 2D manner. One is the *sharp interface model* that attempts to model the void surface as a sharp interface between the conductor material and empty space in the void. This method requires a tracking and accurate book-keeping of the surface elements and their geometry, and hence it is cumbersome. However, it is able to explain some experimental observations well.

The other method is the *phase field model*. This model defined the level of the presence of the conductor material based on a phase field scalar variable.

The value of the variable defines the phase of the material at any point on a fixed grid that defined the simulated specimen. The transition from metal material to an empty void is not sharp as modeled by the first approach, but gradual in terms of the presence of the material. It requires less book-keeping and seems to be more computationally efficient.

2.1.2.2.1 Sharp Interface Model

In 1994, Arzt et al. [24] published their work on the investigation of the behavior of EM-induced voids in narrow, unpassivated aluminum interconnects. Experimentally, it was found that the fatal voids have a specific asymmetric shape with respect to the electron flow direction. They proposed, to the best of our knowledge, the first model which attempted to simulate the void shape changes on the basis of atomic diffusion along the void surface. In their model, they considered an isolated 2D void which extends through the thickness of the line, and atomic diffusion on the void surface was assumed to be the primary transport mechanism. Depending on the balance of the arriving and departing atoms at each point on the surface, the movement and the shape change of a void, in the line was tracked as shown in Fig. 2.4.

The driving forces for such a behavior were modeled using the surface mass flux through a surface element; and they considered two types of mass fluxes as follows

$$I_s^j = -\frac{\delta D_s}{\Omega k T} e Z^* \rho j_s \quad (2.26)$$

$$I_s^{\kappa} = \frac{\delta D_s \gamma}{k T} \frac{\partial \kappa}{\partial s} \quad (2.27)$$

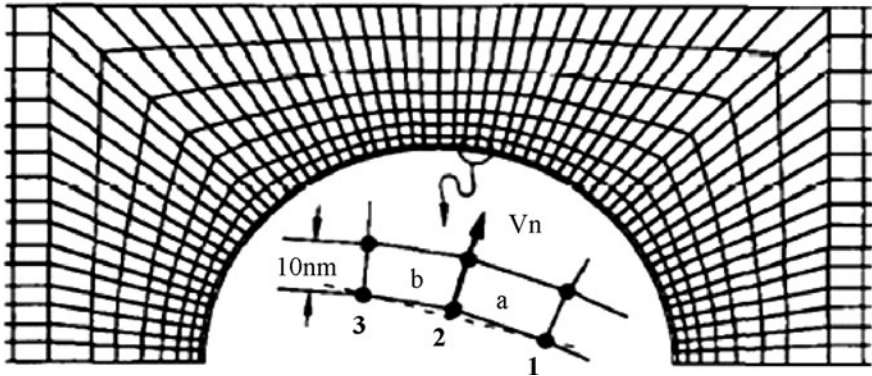


Fig. 2.4 The finite element analysis for a sharp interface model. Reprinted from Kraft and Arzt [25], copyright © 1997, with permission from Elsevier

where I_s^j and I_s^k are the mass fluxes along the surface due to the electron wind force and the curvature of the surface, respectively, δ is the film thickness, D_s is the surface diffusivity, Ω is the atomic volume, k is the Boltzmann constant, T is the absolute temperature, e is the charge of an electron, Z^* is the effective valence, ρ is the resistivity, j_s is the current density along the surface, γ is the surface tension, κ is the curvature, and s is the arc length along the surface.

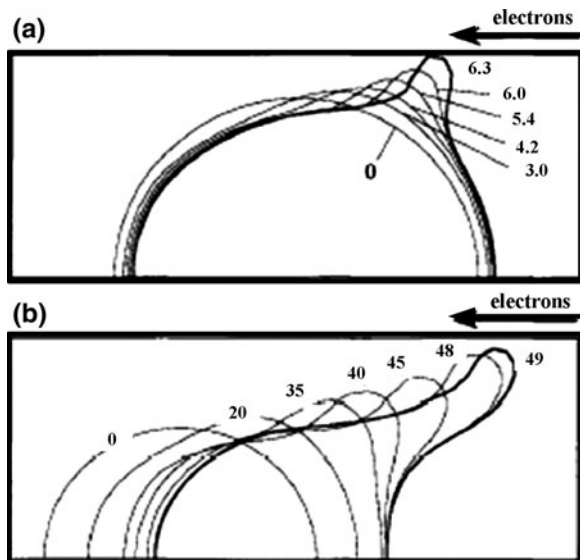
In their model, the current density distribution was calculated based on the assumption of a steady flow of an incompressible, non-viscous, circulation-free liquid, of which the expressions are mathematically identical to the equations of electrostatics. With the knowledge of current density and mass fluxes, the normal velocity at each point of the surface can be computed and the resulting equation of motion of the void surface can be obtained as

$$v_n = \Omega \frac{\partial (I_s^j + I_s^k)}{\partial s}. \quad (2.28)$$

However, with their methodology, the inhomogeneous current distribution in the interconnect around the void was not considered in their model. This non-uniform current density distribution produces temperature gradients, and thus results in local changes in the resistivity and diffusivity. These effects are important for the electromigration failure mechanism in narrow interconnects.

The simulation methodology was thus further modified in their subsequent report [25]. A FEM was used in the calculation of the current density and the temperature distribution. A finite difference method was employed for the void motion and the shape changes computation. Figure 2.5 shows some of their simulation results of the void motion and the shape changes in an Al metal line.

Fig. 2.5 Simulation of the development of initially semi-circular voids with radius of **a** 0.8 μm , **b** 0.6 μm in a 1 μm wide Al metal line. Reprinted from Kraft and Arzt [25], copyright © 1997, with permission from Elsevier



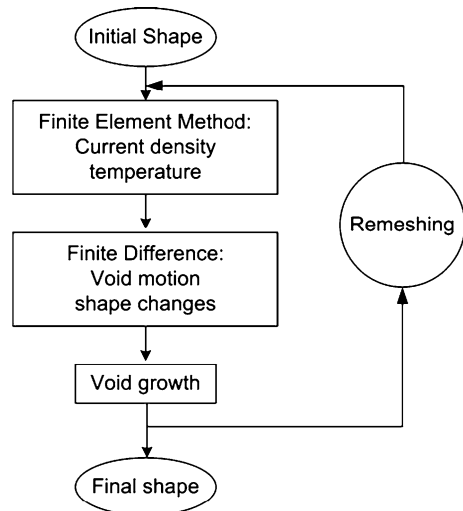
The commercial finite element software ANSYS was used in their modeling. Also included in their work was the consideration of the crystallographic orientation leading to a surface diffusivity change for different angles of the surface with respect to the crystal. To model this effect, they incorporated the anisotropy of the surface diffusivity in the finite element analysis by describing the surface diffusivity as a function of the angle θ between the surface tangent and the conductor line length direction.

In their study, they found that slit voids formed within the grains are likely to be caused by EM-induced surface diffusion. Under sufficiently high current density, a rounded void is unstable and will spontaneously collapse into a slit. The procedure used by Kraft et al. [25] is shown in Fig. 2.6 where an initial void shape is defined, followed by the computation of the current density and temperature due to Joule heating, then the calculation on the shape changes of the void surface. Thereafter, a re-meshing is needed for the modified structure, and the process repeats itself. With this procedure, void shape evolution and shape stability with different void geometries can be studied, and the model has the potential of predicting the lifetime of metal line with certain void shape.

Another similar model was proposed by Wang et al. [26]. In their early studies [27, 28], they showed that atomic diffusion on the void surface, driven by the electrical current, can cause a circular void to translate into a slit void. During this translation process, two forces compete in determining the void shape; one is the surface tension force and the other is the electron wind force due to the electrical current. Surface tension force favors the formation of a rounded void, while electrical current favors a slit void; a rounded void will collapse and become a slit when the electron wind force dominates.

In their later published work [26], they reviewed the experimental and theoretical findings, and provided a numerical simulation of the void shape change.

Fig. 2.6 The flowchart of numerical simulation of the void shape change. Reprinted from Kraft and Arzt [25], copyright © 1997, with permission from Elsevier



Similar to the Kraft's model, they adopted the sharp interface approach and assumed that the void shape change was due to the surface diffusion only, considering all other transport processes as negligibly slow during the void shape change. This approach utilized the same equations as in Kraft's model [24] to model the mass transport. By approximating the void perimeter by many short straight segments, they formulated a finite element procedure for the shape evolution, as done by Kraft [24].

The difference between the above-mentioned two models lies in the implementation of the physical system analysis. Wang et al. used a conformal mapping technique to determine the electric field around the circular void. After that, the electric potential and the curvature of the void surface were determined, and then the Galerkin method [29] was used to determine the EM kinetic system. The Galerkin method will be elaborated in Chap. 3. As a result, their model is capable of modeling void and surface evolutions, and their results are similar to that obtained by Kraft et al. [25]. Compared with the FEM by Kraft, Wang's approach, while mathematically elegant, is not versatile and is hard to yield more complex geometry evolutions [30]. Other similar works were reported by Gungor and Maroudas [31, 32] and Schimschak and Krug [33].

In the sharp interface models developed by many, the common assumption is that the atomic surface diffusion is the dominant diffusion mechanism, and the surface diffusion is driven by the electron wind force and the surface tension force due to the curvature of the void surface only. The anisotropy of the void surface diffusivity is emphasized, and slit voids will only form in grains with certain crystallographic orientations. They studied moving boundary problems entail explicit tracking of the boundary. The interface is described by specifying a large number of points on it. The same equations were used by them to model the atomic surface diffusion and the motion of the void surface at each interface point.

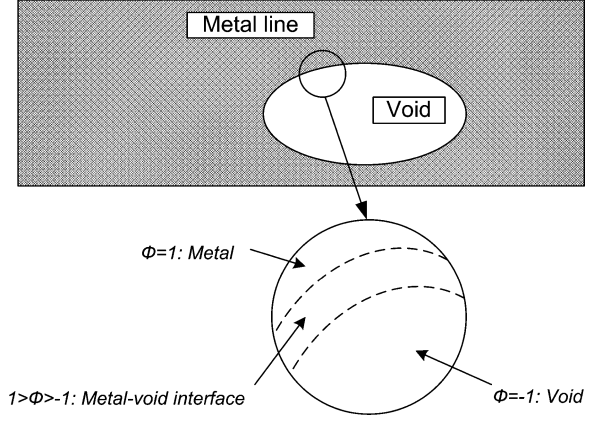
2.1.2.2.2 Phase Field Model

In the Sharp interface model, a lot of interface points are required to accurately describe the void surface when the void shape is evolving, and the changing boundary conditions must be implemented at this increasingly numerous set of points. Thus, the sharp interface model can get very complicated and also tends to have rather poor numerical stability [34, 35].

On the other hand, if the entire domain is described by a continuously varying scalar order parameter ϕ which has a value of +1 for region well within the metal "phase" and -1 for region well within the void "phase", and ϕ has a value between +1 and -1 for the metal-void interface as shown in Fig. 2.7, we have the phase field model [36].

This model was introduced independently by Fix [37] and Collins and Levine [38], and it received considerable attention in the context of phenomena associated with evolving interface. The earliest attempt to use the phase field model for the line

Fig. 2.7 The void simulation in a phase field model



interconnect failure simulation was reported by Mahadevan and Bradley [35]. In their study, they simulated the time evolution of a perturbation to the edge of a current carrying, single-crystal, unpassivated metal line. Surface electron wind force migration, surface self-diffusion due to the current crowding, and the curvature of the void surface were all taken into account. They adopted the same formula that model the diffusion mechanisms along the void surface used by Kraft [24], but the idea of a sharp interface between metal and void was abandoned. The inclusion of the phase field model results in two coupled partial different equations, with the first one describing the dynamics of the phase field, and the second one describing the electric field as given below.

$$-\varepsilon \frac{\partial \phi}{\partial t} = \vec{\nabla} \cdot \left\{ \alpha_0 \left[1 + \lambda_s \varepsilon \left(\vec{\nabla} \phi \right)^2 \right] \vec{\nabla} v - \left[\varepsilon^2 \beta_0 (\phi + 1) \left(\vec{\nabla} \phi \right)^2 \vec{\nabla} \Phi_E \right] \right\} \quad (2.29)$$

$$\alpha_0 = \frac{3M_0 \lambda_s \Omega}{D_s L}, \quad \lambda_s = \frac{3D_s h}{M_0 L k_B T}, \quad \beta_0 = \frac{3Z_s^* e E_0 h}{k_B T} \quad (2.30)$$

$$v = \varepsilon^2 \nabla^2 \phi + g(\phi), \quad g(\phi) = (\phi - \phi^3)/2 \quad (2.31)$$

and

$$\vec{\nabla} \cdot \left[\sigma(\phi) \vec{\nabla} \Phi_E \right] = 0 \quad (2.32)$$

where D_s is the surface diffusivity and L is a characteristic length describing the void which can be taken to be the square root of the void surface area. Φ_E is the electrical potential, ε is a dimensionless constant proportional to the interface width, M_0 is the lattice diffusivity of the phase field, k_B is the Boltzmann constant, λ_s is the surface tension, T is the temperature, and σ is the conductivity.

The phase field model was used for an isolated void in an infinite thin film, and this method can be easily extended so that it applies to the time evolution of an edge perturbation in a metal line of finite extent. By solving the phase field equations and

the electric field equations numerically, the model provides the time evolution of a small notch at the edge of a current-carrying single crystal metal line [35]. The model is able to predict a threshold value of the applied current so that the edge perturbation will grow into a slit-shaped void that spans the wire. Mahadevan and Bradley also explained the physical origin of this instability and pointed out the importance of the crystalline anisotropy and mass transport along the edge of the line.

At nearly the same time as Mahadevan and Bradley, Bhate et al. [39] reported their own version of the phase field model for simulating the process of electron wind force migration, curvature-driven surface migration, and the stress-driven migration. In their work, Bhate et al. [39] briefly discussed the theory of the sharp interface model and its limitations and disadvantages. They then proposed their own phase field model. Their approach is based on the introduction of an order parameter field to characterize the damaged state of an interconnect. The order parameter takes on distinct uniform values within the material and the void, varying rapidly from one to the other over narrow interfacial layers associated with the void surface. They derived the field equations for the order parameters based on the microforce balance principle of Gurtin [40].

Accordingly, they expressed the free energy of the line as

$$\mathbb{F}(\phi, \varphi) = \int_R F(\phi, \nabla \phi, \varphi) dV = \int_R \left\{ \frac{2\gamma_s}{\varphi\pi} \left(f(\phi) + \frac{1}{2} \varphi^2 |\nabla \phi|^2 \right) + W(\varphi, \phi) \right\} dV \quad (2.33)$$

where $f(\phi)$ is the bulk free energy, γ_s is the isotropic surface energy, φ is a parameter that controls the thickness of the interfacial layer associated with the void surfaces, and W is the elastic strain energy. The atomic diffusion paths through the bulk and grain boundary were assumed to be negligible, and the only mode of transport for atoms was the diffusion along the void surfaces in their model. This is the same assumption as in most sharp interface models, except that the surface diffusivity in their model was treated as isotropic. However, this assumption is not justifiable since it has been proved that the anisotropic diffusivity of atoms along the void surface has a strong effect on the evolution of void during EM [24].

2.1.3 Summary

From the above discussion, all the 1D EM models are focused on the simulation of the EM kinetics. The kinetics of EM, such as the EM driving forces due to electron wind force and vacancy concentration and stress gradients, were simulated through the calculation of the change in vacancy concentration along the metal line. From the evolution of the vacancy concentration, the critical location of the metal line can be identified, and the time to failure can be extracted if reasonable criterion of failure is given.

The 1D EM modeling is capable of integrating the multiple driving forces to simulate the kinetic of EM process and evaluating the impact of the properties of

the metal line on the EM performance, such as the length, the passivation layer, and the various boundary conditions that represent the interconnect structures in a simplified manner. However, the real EM process in a metal line is rather complicated. 1D EM modeling is only capable of simulating the simplified scenarios of EM due to its limitation on dimensionality. The influence of the triple points of the multiple grain textures, the surrounding materials and the induced thermo-mechanical stress, the shape of the metal line or the microstructure of the interconnects were poorly addressed in the 1D modeling. The consideration of the EM from thermodynamics aspect, such as the various diffusion paths for atoms diffusion, was highly simplified in the 1D model.

Unlike the 1D EM models, 2D EM models are able to consider the effects of microstructure of interconnects and the surrounding material on the EM performance. However, the difficulties and complexities in the mathematical implementation increase dramatically as the coupled partial differential equations have to be solved in multiple dimensions. Rather than tracking the vacancy concentration evolution of a 1D metal line, most of the 2D EM models are based on the formulation and calculation of the atomic flux due to various driving forces and along various diffusion paths in the metal line. The typical EM-driving forces include electron wind force, atomic concentration gradient, temperature gradient, stress gradient and surface tension. The typical EM diffusion paths include interface diffusion, grain boundary diffusion, and lattice diffusion inside a grain. Numerical method, such as finite element analysis, is needed to solve the EM equations in a coupled manner with current density, temperature, and stress distributions.

Most of the proposed 1D and 2D models investigate the EM within the interconnect material itself, and the effect of the surrounding materials on the interconnect EM is not taken into consideration. However, as the interconnect line width goes into 150 nm and below, and with the use of the low- k dielectric, the impact of the surrounding materials on the interconnect EM becomes significant. The thermal conduction and the mechanical stiffness of the dielectric materials surrounding the interconnect structure play a major role in determining the EM reliability of an interconnect system. In other words, EM studies can no longer be limited to the interconnect material itself, and one needs to consider the entire interconnect system. Such a study will require a 3D EM simulation. A more detailed discussion on the application of finite element analysis for EM simulation in 3D manner will be given in [Chaps. 3 and 4](#) of this book.

2.2 Review on the Modeling of the Stress-Induced Voiding (SIV)

Stress-induced voiding is another serious reliability challenge to IC interconnects for both the Al- or Cu- based metallization. Large thermo-mechanical stress is developed in interconnects during fabrication and cooling to room and operating

temperatures, and this initiates stress relaxation and give rise to SIV. The physical mechanism of the stress development and relaxation have been studied [41, 42]. For example, chip with electroplated Cu interconnects consists of small grains initially. If the lines are not annealed properly before encapsulation, subsequent annealing will cause grain growth, resulting in grain growth-induced stress in the line [43]. The stress-induced voids can deteriorate the EM lifetime of an interconnect as observed experimentally [44].

The failure site varies in interconnects under thermo-mechanical stress. Ogawa et al. reported SIV void formation under via due to grain growth without thorough annealing [45]. The void in via in the form of copper pull up is attributed to poor interface adhesion in Cu/FSG interconnects [46]. Hommel et al. also reported SIV voids along via side walls and via bottom for Cu interconnects [47]. In the experimental work by An and Ferreira [48], dislocation was observed in wide interconnect while SIV void was formed in narrow interconnects. Via deformation was also observed in Cu/SiLK line-via structure [49]. In fact, the type and location of the failure is strongly dependent on the interconnect geometry, dielectric type, as well as the microstructure of the interconnects.

Conventional stress measurement methods such as wafer curvature measurements [50, 51], analytical modeling [12], and X-ray diffraction (XRD) methods have been developed to analyze the stress distribution in interconnect systems [52]. However, these methods are limited to simple test structures and they can only determine the average stress in the interconnect. On the other hand, FEM can be performed to determine the stress condition of complex multi-level structures [53, 54]. In this section, we will present a comprehensive review on the physics-based SIV modeling in the past two decades. The review focuses on four categories: (1) thermo-mechanical stress modeling; (2) analytical modeling; (3) vacancy and atomic migration modeling; and (4) stress-induced migration modeling. Each category provides a unique perspective to help us understand the SIV phenomenon in interconnects.

2.2.1 Thermo-mechanical Stress Modeling

The characteristics of thermo-mechanical stress in interconnects depend on how effective the Si substrate and the dielectrics confine the metal interconnect from expanding freely. Therefore, the thermo-mechanical properties of the dielectrics and the geometry of the structure can affect the magnitude and nature of the thermo-mechanical stress greatly. Compared with SiO₂, low-*k* materials are expected to have poorer mechanical properties and this can lead to severe stress-related problems in low-*k* interconnects [55].

Hydrostatic stress and von Mises stress are two important quantities in studying the stress-induced failure in interconnects. The hydrostatic stress σ_H and von Mises stress σ_V are given as [56]

$$\sigma_H = \frac{\sigma_1 + \sigma_2 + \sigma_3}{3} \quad (2.34)$$

$$\sigma_V = \frac{1}{\sqrt{2}} \left[(\sigma_1 - \sigma_2)^2 + (\sigma_2 - \sigma_3)^2 + (\sigma_3 - \sigma_1)^2 \right]^{1/2} \quad (2.35)$$

where σ_1 , σ_2 , and σ_3 are the principal stresses in the line along the stress orthogonal cartesian coordinates.

Hydrostatic stress is proven to be the driving force for void nucleation [57]. On the other hand, von Mises stress, which is normally used as a criterion for evaluating deformation, does not result in the volumetric changes of the material [58]. At the early stage of a typical SIV process, under the constraint of the surrounding materials, the shear stress in an interconnect is relaxed through either diffusion creep or dislocation glide [59, 60], causing the interconnect to be at a near perfect hydrostatic state. During the subsequent void-growing process, the duration of plastic deformation is found to be much shorter than the duration of the hydrostatic stress relaxation [59], and von Mises stress can therefore be neglected. In fact, a gradient in hydrostatic stress can still exist after plastic deformation, which induces SIV subsequently [61].

In the work of Rhee et al., stress behavior of blanket Cu films were studied through both X-ray diffraction method and FEM [53]. With the help of the FEM, the effects of scaling, barrier thickness, and low- k dielectrics were studied in their work. It was found that the hydrostatic stress normal to the surface increase with decreasing line width while the stress along the line did not change much with line width. Besides, the severity of SIV formation in low- k interconnect is reduced due to lesser confinement effect by the surrounding dielectrics. This is due to the fact that the effective bulk modulus is much smaller for low- k interconnects than that of SiO₂-based interconnects as is also reported in the work of Hou and Tan [62] using

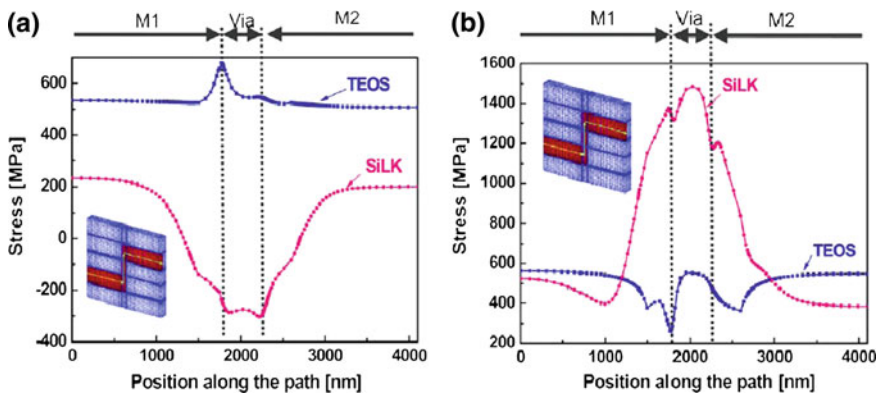


Fig. 2.8 Stress variation from M1 to M2 along the path for the TEOS-embedded and the SiLK-embedded structures. **a** Hydrostatic stress, **b** von Mises stress. Reprinted from Paik et al. [56], copyright © 2004, with permission from Elsevier

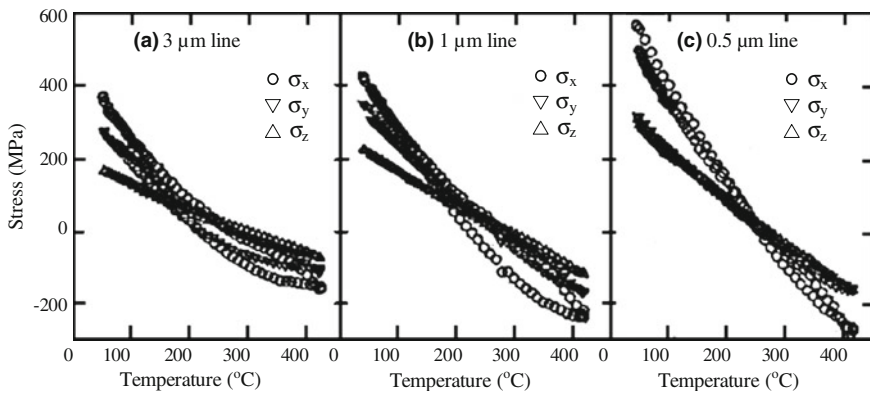


Fig. 2.9 Stress versus temperature curve of passivated Al(Cu) lines for **a** 3 μm wide, **b** 1 μm wide, and **c** 0.5 μm wide lines, respectively [59], copyright © 1995 IEEE

FEM. On the other hand, the increases in the von Mises stress in low- k interconnect raises the reliability concern for interfacial delamination or plastic deformation in low- k passivated lines [53].

The stress state in M1-via-M2 structures is studied by Paik et al. [56] using FEM. Two extreme cases were considered in their work, namely TEOS- and SiLK as dielectrics respectively. The hydrostatic stress and von Mises stress distributions along M1, via and M2 for TEOS and SiLK-based interconnects are shown in Fig. 2.8a, b respectively. It was noted that the von Mises stress of the SiLK structure was much higher than that of the TEOS structures in the via, although the von Mises stresses in the M1 and M2 lines of SiLK structure were similar to those of TEOS structures as shown in Fig. 2.8b. This implies that the stress state of via is significantly different from that of lines and deformation will occur mainly in the via and not in the lines. Similar modeling work can also be found in other references [55, 63].

The scaling effect on the thermo-mechanical stress in interconnect was addressed in the work of Ho et al. through beam bending measurement [59]. It was found that with decreasing line dimensions, the confinement due to the surrounding materials was enhanced and the stress level was increased sufficiently to cause void formation. In their bending beam measurement experiment, Al line with line width of 3, 1 and 0.5 μm were subjected to thermal cycling from room temperature to 400°C. The lines behaved more elastic with less stress hysteresis during thermal cycling with smaller line width as shown in Fig. 2.9. With decreasing line width, the difference in the magnitude of the stress components decreases, making the stresses more hydrostatic. For the stress relaxation behavior, the rate of stress relaxation along the line was the fastest, followed by the stress component across the line and then the stress normal to the line.

Compared with FEM, analytical modeling of stress components is more useful to extract quick estimates and to gain a greater insight into the mechanics and physics of the stress evolution. The early analytical models were based on the

Eshelby theory of inclusions in which the line was modeled as an ellipsoidal cylinder embedded in an infinite isotropic matrix of the passivation material [60, 64]. However, these models did not capture the interaction between neighboring lines as well as the elastic properties of the substrate or sharp edges of the line. These two limitations were later overcome by Wikstrom et al. [65] and the analytical modeling results were found to be consistent with the FEM calculations.

2.2.2 Analytical Modeling of SIV

Pre-existing micro-voids were found in both wide and narrow Cu interconnects under thermo-mechanical stress before electromigration (EM) test [66]. These microvoids can grow during EM and become fatal voids at the cathode end of an interconnect [44]. Shen et al. found that a large stress-induced void was more prone to growth during subsequent EM test [67]. Many studies have been carried out to investigate SIV from different perspectives such as the quality of passivation layer [68], the mechanical strength of interlayer dielectrics (ILD) [53], the microstructure of the film [69], and they were indeed found to affect the thermo-mechanical stress in metallization and hence its SIV lifetime. Detailed information of such factors is incompletely known however, and will probably never be precisely controlled in fabrication. There is no single model that accounts for all the aspects of SIV. Therefore, it is desirable to consider the physics of the phenomenon semi-quantitatively and different analytical models will be discussed here.

2.2.2.1 Saturate Void Volume

An encapsulated metal line is stress free at high temperature T_0 , and it is commonly known as stress free temperature (SFT). As the total number of atoms in the line is constant at all time, when the line is cooled down to storage temperature T , the thermo-mechanical stress is generated due to the mismatch in the coefficient of thermal expansion (CTE) of the interconnect and the surrounding materials. Void space is then created in order to release the resulting stress, and upon complete relaxation, the void volume will be saturated. The saturated void volume (V_{SV}) is given by Suo [70]

$$V_{SV} = 3 \cdot \Delta\alpha \cdot (T_0 - T)V \quad (2.36)$$

where V is the volume of the metal line and $\Delta\alpha$ is the effective thermal expansion mismatch strain, i.e., the difference in the CTE between the metal line and its surrounding materials. For silica-based interconnect structure, since the metals have much larger CTE than that of the surrounding materials, we can use the CTE of Cu in the estimation. Using the typical values of $18 \times 10^{-6}/K$ for $\Delta\alpha$ and 300 K for $(T_0 - T)$ [70], the void volume fraction is evaluated to be 1.62% for Cu interconnects.

2.2.2.2 Void Initiation

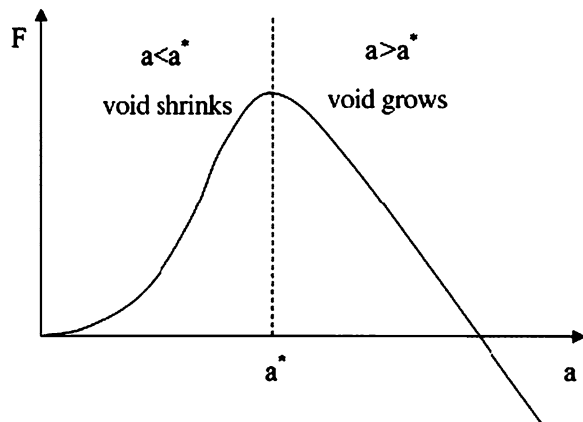
Within the context of continuum mechanics, SIV is one of the means to release the stored strain energy of an interconnect system by mass redistribution. Considering a tiny void in a metal line under thermo-mechanical stress, the void can change its size by relocating atoms on its surface to area in the metal far away from the void under stress gradient-induced driving force. In this process, the void increases its surface area and hence the free energy increases. During this process, work is done by the thermo-mechanical stress, reducing the free energy of the system.

Considering interconnects without tiny void under the thermo-mechanical stress as the ground state, the system has zero free energy. Now, the current state has a void of radius a . Assuming the void is in spherical shape, and let γ be the surface energy per unit area. By creating the void, a surface of area of $4\pi a^2$ is exposed, raising the free energy of the system by $\gamma 4\pi a^2$. At the same time, atoms occupying the volume of $4\pi a^3/3$ is relocated from the void, allowing the remote stress to do the work by $\sigma 4\pi a^3/3$. Thus, the free energy of the system, relative to that of solid with no void is

$$F(a) = 4\pi a^2 \gamma - \frac{4}{3} \pi a^3 \sigma \quad (2.37)$$

Figure 2.10 shows the free energy as a function of the void radius. Based on Eq. 2.37, the critical void radius is given by $a^* = 2\gamma/\sigma$. One can see from Fig. 2.10 that when the void is small, the surface energy dominates, and the void will shrink to reduce the free energy, rendering no void formation after some time. When the void is large, the stress dominates, and the void will grow to reduce the free energy. The critical void radius a^* exists when the free energy is maximum. Using typical values of 1 J/m^2 for γ and 200 MPa for σ in Al(Cu) material [71], the critical radius is evaluated to be 10 nm . Such void size is used in the work of Hou and Tan for the simulation of thermo-mechanical stress in the presence of the mini-void [71].

Fig. 2.10 The free energy as a function of radius. Reprinted from Suo [70], copyright © 2003, with permission from Elsevier



2.2.2.3 Lifetime Formulations

The stress evolution during SIV can be described by the following [72, 73],

$$\frac{\delta \sigma_H}{\delta t} = K \nabla^2 \sigma_H \quad (2.38)$$

where t is the time, σ_H is the local hydrostatic stress driving the mass transport, and K is the effective diffusivity defined as $K = \frac{DB\Omega}{k_B T}$. Here, D is the atomic diffusivity, Ω is the atomic volume, k_B is the Boltzmann's constant, T is the local temperature, and B is the effective bulk modulus which describes the confinement effect of the surrounding materials on the metal line. Equation 2.38 governs the stress evolution in interconnects. The analytic solutions of Eq. 2.38 for 1D and 2D line structures can be found in the works from Zhai and Blish [73]. For the case of 1D, it is given as

$$\sigma(x, t) = \frac{2\sigma_0}{m_n} \sum_{n=0}^{\infty} \exp(-Km_n^2 t / L^2) \sin\left(\frac{m_n}{L}x\right) \quad (2.39)$$

Equation 2.39 represents the analytical stress solution for 1D line structure where $m_n = (2n + 1)\pi/2$ and L is the length of the interconnect. This 1D model represents the intermediate and later stage for a typical SIV process where the diffusion length is much larger than the line width.

For a 2D line structure, the solution of Eq. 2.38 is given as

$$\sigma(r, t) = \sigma_0 \cdot \text{erf}\left(r/\sqrt{4Kt}\right) \quad (2.40)$$

Equation 2.40 is the analytical stress solution for 2D line structure where $r = 0$ is the origin or the void nucleation site. This 2D model represents the early stage of SIV where the diffusion length is shorter than the line width.

Equations 2.39 and 2.40 form a simplified stress evolution model for SIV, which contains some of the most fundamental perspectives including effective diffusivity, line length, time, and initial stress.

Assume an initial flaw exist in a metal line and is large enough that the stress near the flaw is zero. In this case, Eq. 2.38 is identical to the usual diffusion equation with K acts as the diffusivity. The solution to this initial-boundary value problem is well known, and the time for a void to relax a segment of interconnect of length l is [70]

$$t_l \sim \frac{L^2 kT}{DB\Omega}. \quad (2.41)$$

Assume a void length of L constitutes the failure, the SIV lifetime is approximated as [70]

$$t_{life} \propto \frac{1}{B[(\alpha_m - \alpha_d)(T_0 - T)]^2} \exp\left(\frac{E_A}{k_B T}\right). \quad (2.42)$$

This effective bulk modulus B is dependent on the cross section of the interconnect as well as dielectric materials, and one can therefore infer from Eq. 2.40 that a structure with a smaller B will lead to a longer SIV lifetime, if other things being the same.

Fischer et al. proposed another model to formulate the SIV lifetime [47, 74]. Their derivation was based on the assumption that the change in the plastic strain leads to an increase of the void volume which is proportional to the increase of the line resistance. With this assumption, they derived the median time to failure (MTF) for SIV as follows

$$t_{life} \propto C \frac{T}{T_0 - T} \exp\left(\frac{E_A}{kT}\right) \quad (2.43)$$

where C is independent on temperature and represents a specific constant for a set of identical test structures.

The temperature exponents in Eqs. 2.42 and 2.43 are different, and different temperature exponent can lead to a deviation of the estimated activation energy. In the recent work by Hou et al. [71], the SIV lifetime formulations were derived from the energy perspective. They found that the temperature exponent in the SIV lifetime formulations was determined by the available diffusion paths for the interconnect atoms and the interconnect geometry. Based on the diffusion pathways available, they classified the SIV process into three categories as linear, square, and cubic as shown in Fig. 2.11a–c.

The generalized expression for the SIV lifetime is expressed as [75]

$$t_{life} \propto C \frac{T}{(T_0 - T)^N} \exp\left(\frac{E_A}{k_B T}\right) \quad (2.44)$$

where N is the temperature exponent depending on interconnect geometry and microstructures and C is independent on temperature. N is equal to 4, 2, and 4/3 for the linear, square and cubic cases respectively.

Equation 2.44 implies that the failure time approaches infinity when SIV test is carried out at either the SFT T_0 , or the absolute 0 K. As the test temperature increases from 0 K, the tensile thermo-mechanical stress decreases linearly and the

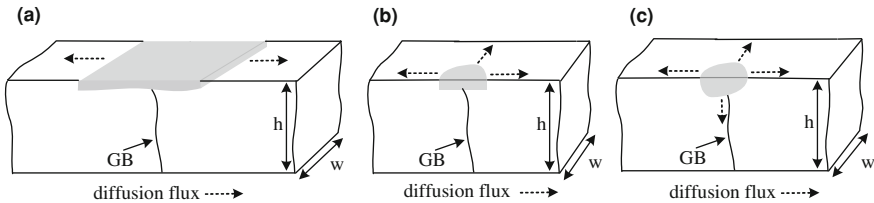


Fig. 2.11 Three cases of stress relaxation volume evolution are indicated by the grey area. The relationship between the stress relaxation volume and diffusion length is categorized as **a** linear, **b** square, and **c** cubic. Reprinted with permission from Tan and Hou [75], copyright © 2007, American Institute of Physics

diffusivity increases exponentially. As a consequence, the SIV lifetime decreases with temperature up to a critical point, above which the lifetime increases with increasing temperature. Therefore, to maximize acceleration in reliability test, SIV should be performed around T_{crit} . This T_{crit} can be determined by differentiating Eq. 2.44 with respect to T , and we have

$$T_{\text{crit}} = \frac{2E_A T_0}{\sqrt{(E_A - k_B T_0)^2 + 4E_A T_0 k_B N + E_A + k_B T_0}}. \quad (2.45)$$

Equation 2.45 reveals that T_{crit} is dependent on the activation energy, temperature exponent, and SFT.

Compared with the work of Ogawa et al. [76], where E_A was given as 0.74 eV and T_0 was found to be 270°C, T_{crit} is evaluated to be within 172–228°C using Eq. 2.45 for the different value of N used, and the computed T_{crit} agrees well with their experimental observations of 190°C. In the recent work of An et al. [48] where the grain boundary diffusion was found to be as important as the interface diffusion, we use the temperature exponent of 4/3 for Eq. 2.45 with E_A at 0.74 eV as in the previous case, the critical temperature evaluated from Eq. 2.45 is around 255°C, in good agreement with the experimentally observed 250°C. For Al interconnects, Fischer et al. also reported the similar critical temperature for Al interconnects at slightly higher activation energy [74].

2.2.3 Vacancy and Atomic Migration Model

SIV phenomenon occurs during storage test for long periods and is accelerated at high temperature storage. Numerous vacancies are generated thermodynamically in the metal interconnect at high temperatures, and they migrate due to the stress gradient and accumulate at vacancy sinks in the interconnect. The accumulation of the vacancies leads to the formation of voids. Based on the fact that vacancy migration and void growth are enhanced by the thermo-mechanical stress, stress-induced vacancy model was proposed in Aoyagi's early work [77]. In his work, the vacancy distribution was directly correlated with the thermo-mechanical stress distributions based on the stress-induced vacancy model, and the thermo-mechanical stress distribution was simulated using FEM. The SIV weak point was predicted to be near interconnect sidewalls and it was in qualitative agreement with the experimental results for Al interconnects.

The temperature characteristics of SIV was studied through the model of Aoyagi [78]. The vacancy concentration C under stress is given by Flinn [57],

$$C = \exp\left(-\frac{E_F}{k_B T}\right) \exp\left(\frac{S_F}{k_B}\right) \exp\left(\frac{\sigma \Omega}{k_B T}\right) \quad (2.46)$$

where E_F is the single-vacancy formation energy, S_F is the single-vacancy formation entropy, Ω is the vacancy volume, and σ is the stress which is defined to be positive for tensile stress. Here, the vacancy concentration C is defined as the ratio of the number of vacancies to the number of atoms constituting the metal.

When vacancy sinks (e.g. defects) exist in the interconnect under tensile stress, the vacancies migrate to the vacancy sinks. The driving force of the migration of vacancies is the difference of the stresses on the void surface which is zero and the residual thermo-mechanical stress in the interconnect. Aoyagi's study revealed that the temperature characteristics of the vacancy flux has a peak at a certain temperature which changes due to stress relaxation [78].

Later on, Aoyagi also performed numerical simulation to evaluate the resistance change in interconnect during the SIV process [79]. He considered a simplified slit-like void as shown in Fig. 2.12. The atomic migration model was based on the migration of atoms due to the thermo-mechanical stress gradient present in interconnects.

The atomic flux J in the SIV process can be expressed as [79]

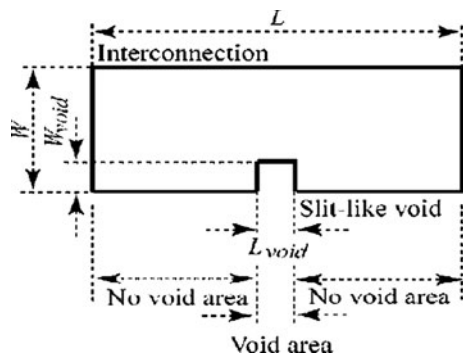
$$J = \frac{D}{k_B T} N_{\text{atom}} \nabla(\sigma \Omega) \quad (2.47)$$

where D is the atomic diffusion coefficient, N_{atom} is the number of atoms, Ω is the atomic volume, and σ is the thermo-mechanical stress which is defined to be positive for a tensile stress. In general, the diffusion coefficient is enhanced at a higher temperature or under a tensile stress as given by Aoyagi [79]

$$D = D_0 \exp\left(-\frac{E_m}{k_B T}\right) \exp\left(\frac{\sigma \Omega}{k_B T}\right) \quad (2.48)$$

where E_m is the activation energy for the self-diffusion of atoms and D_0 is the diffusion constant. The relationship between resistance change, storage temperature, storage time, and void width is shown in Fig. 2.13a–d. We can see that the interconnects disconnect suddenly after a certain storage time, depending on the storage temperature.

Fig. 2.12 Top view of an interconnection with a slit-like void for the simulation. Reprinted from Aoyagi [79], copyright © 2006, with permission from Elsevier



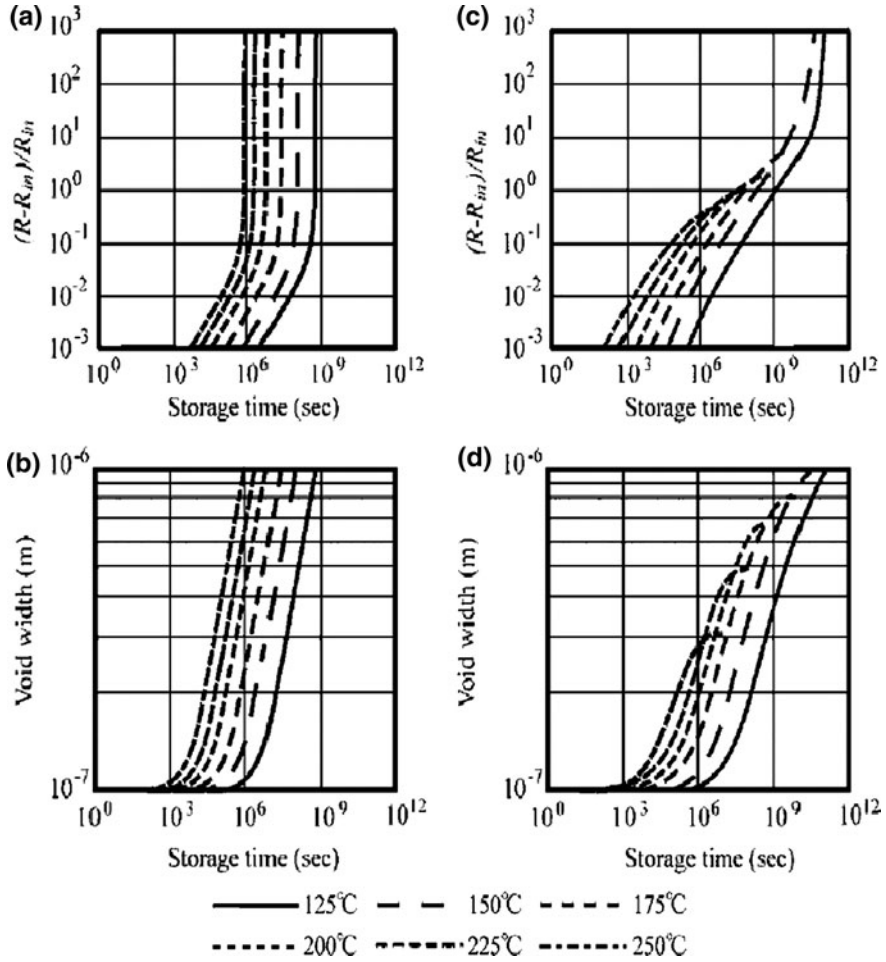


Fig. 2.13 Change in the line resistance and void width as a function of storage time for aluminum interconnect with the storage temperature as a parameter. **a, b** The void is 1 nm long and 100 nm wide in its initial stage. **c, d** The void is 50 nm long and 100 nm wide in its initial stage. Reprinted from Aoyagi [79], copyright © 2006, with permission from Elsevier

2.2.4 SIV for Nano-interconnects

Replacing SiO_2 with low- k materials results in a decrease of the tri-axial stress in Cu [80]. However, it is still under debate whether the SIV performance for low- k interconnects improves or degrades when compared with that in SiO_2 -based interconnects. Bruynseraede et al. [81] stated that SIV shall improve due to a lower density of nano-defects generated by the plastic deformation in low- k interconnects. Suo [82] also reported that low- k interconnect should be more SIV

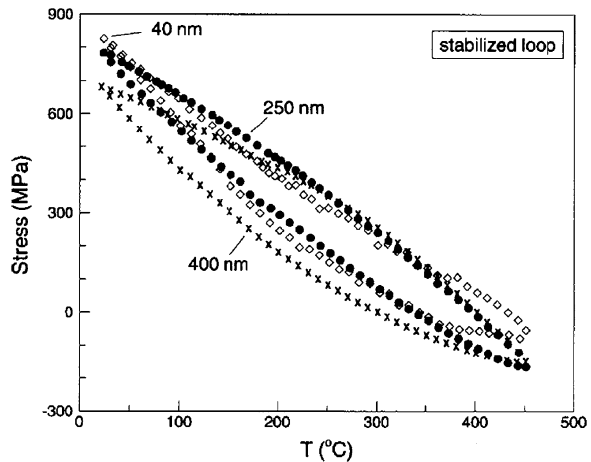
resistant due to a reduced effective bulk modulus. However, Gan et al. [83] demonstrated that low- k interconnects suffered more from SIV at via bottom due to a higher stress gradient despite a lower thermo-mechanical stress.

Based on the recent SIV model proposed by Tan and Hou [75], SIV performance for the low- k interconnects depends on the compromise between the confinement and the passivation effects. Since the passivation condition is highly process dependent, if one can assume that the passivation on Cu surface is the same for both Cu/SiO₂ and Cu/low- k interconnects, Cu/low- k interconnects will outperform its counterpart in SIV due to a lower thermo-mechanical stress. In reality, the passivation condition is poorer for Cu/low- k interconnect as indicated by a lower interface energy for low- k interconnects [84]. In short, the SIV performance for Cu/low- k interconnects is strongly dependent on the process and materials used during fabrication.

When interconnect is scaling down to 0.16 μm , the thermo-mechanical stress will increase slightly as shown by Tan et al. [85] using FEM. Their simulation model is based on the classical continuum mechanics which is intrinsically size independent. However, when the line width is scaled down further into nano-regime, elastic properties of the interconnects become size dependent, and a qualitative departure from classical mechanics is expected. Sharma et al. [86] demonstrated that the thermo-mechanical stress decreases at line width goes below 50 nm by considering the size dependency in elasticity. The finite element analysis incorporating the size-dependent effects are still lacking for interconnects below 100 nm.

Besides the SIV, large von Mises stress in interconnects may also cause reliability problems, particularly for Cu/low- k interconnects. Paik et al. [63] showed that the von Mises stress in low- k interconnects is larger than that of the SiO₂-based interconnect, through finite element analysis. A large von Mises stress within the interconnect system would result in failures in the form of plastic deformation. For instance, via barrier layer cracking is reported by Paik et al. [56]

Fig. 2.14 Stabilized stress–temperature response for passivated Cu films of various thicknesses. Reprinted from Shen and Ramamurty [90], copyright © 2003, with permission from Elsevier



in low- k interconnect due to the high von Mises stress at via region. In fact, owing to the reduced fracture energy of the low- k materials [87], dielectric failure is becoming important for nano-interconnects with low- k dielectric [88].

As line width is scaling down, plastic deformation is less likely to happen due probably to the increased elasticity of the interconnects [89]. The enhancement in elasticity of interconnect was confirmed by Shen and Ramamurty [90] who found that the hysteresis loop becomes smaller with decreasing film thickness during thermal cycling as shown in Fig. 2.14, implying increasing difficulty of plastic deformation. Recently, Budiman et al. [52] also reported that the plastic deformation was less likely to happen in narrower interconnects by synchrotron X-ray microdiffraction measurements.

2.2.5 Summary

Stress-induced voiding is a serious reliability problem in metal interconnects. In this chapter, we review the progress on the physics-based SIV modeling from four aspects, namely the thermo-mechanical stress modeling, analytical modeling, vacancy and atomic migration model, and stress migration for nano-interconnects. Each category provides a unique perspective for us to understand the physics of SIV process.

References

1. Clement JJ (2001) Electromigration modeling for integrated circuit interconnect reliability analysis. *IEEE Trans Device Mater Reliab* 1:33–42
2. Rosenberg R, Ohring M (1971) Void formation and growth during electromigration in thin films. *J Appl Phys* 42:5671
3. Blech IA (1976) Electromigration in thin aluminum films on titanium nitride. *J Appl Phys* 47:1203–1208
4. Blech IA, Herring C (1976) Stress generation by electromigration. *Appl Phys Lett* 29:131–133
5. Shatzkes M, Lloyd JR (1986) A model for conductor failure considering diffusion concurrently with electromigration resulting in a current exponent of 2. *J Appl Phys* 59:3890
6. Kirchheim R, Kaeber U (1991) Atomistic and computer modeling of metallization failure of integrated circuit by electromigration. *J Appl Phys* 70:172
7. Clement JJ, Lloyd JR (1991) Numerical investigations of the electromigration boundary value problem. *J Appl Phys* 71:1729
8. Tu KN (1992) Electromigration in stressed thin films. *Phys Rev B* 45:1409
9. Ross CA (1991) Stress and electromigration in thin film metallization. *Mater Res Soc Proc* 225:35–46
10. Kirchheim R (1992) Stress and electromigration in Al-lines of the integrated circuits. *Acta Metall Mater* 40:309
11. Korhonen MA, Borgesen P, Tu KN, Li C-Y (1993) Stress evolution due to electromigration in confined metal lines. *J Appl Phys* 73:3790

12. Clement JJ, Thompson CV (1995) Modeling electromigration-induced stress evolution in confined metal lines. *J Appl Phys* 78:900
13. Park YJ, Andleigh VK, Thompson CV (1999) Simulations of stress evolution and the current density scaling of electromigration-induced failure times in pure and alloyed interconnects. *J Appl Phys* 85:3546
14. Park YJ, Thompson CV (1997) The effects of the stress dependence of atomic diffusivity on stress evolution due to electromigration. *J Appl Phys* 82:4277
15. Andleigh YK, Fayad W, Verminski M, Thompson CV (eds) <http://nirvana.mit.edu/emsim/>
16. Hau-Riege CS, Thompson CV (2000) The effects of microstructural transitions at width transitions on interconnect reliability. *J Appl Phys* 87:8467
17. Hau-Riege SP, Thompson CV (2000) Electromigration saturation in a simple interconnect tree. *J Appl Phys* 88:2382
18. Hau-Riege SP (2002) Probabilistic immortality of Cu damascene interconnects. *J Appl Phys* 91:2014
19. Tan CM (2010) Electromigration in ULSI interconnection. World Scientific Publishing Co, Singapore
20. Gleixner RJ, Nix WD (1999) A physically based model of electromigration and stress-induced void formation in microelectronic interconnects. *J Appl Phys* 86:1932
21. Sukharev V, Zschech E (2004) A model for electromigration-induced degradation mechanisms in dual-inlaid copper interconnects: effect of interface bonding strength. *J Appl Phys* 96:6337
22. Zschech E, Sukharev V (2005) Microstructure effect on EM-induced copper interconnect degradation: experiment and simulation. *Microelectron Eng* 82:629
23. Zschech E, Meyer MA, Mhaisalkar SG, Vairagar AV, Krishnamoorthy A, Engelmann HJ, Sukharev V (2006) Effect of interface modification on EM-induced degradation mechanisms in copper interconnects. *Thin Solid Film* 504:279
24. Arzt E, Kraft O, Nix WD, Sanchez JJE (1994) Electromigration failure by shape change of voids in bamboo lines. *J Appl Phys* 76:1563
25. Kraft O, Arzt E (1997) Electromigration mechanisms in conductor lines: void shape changes and slit-like failure. *Acta Mater* 45:1599
26. Wang W, Suo Z, Hao TH (1996) A simulation of electromigration-induced transgranular slits. *J Appl Phys* 79:2394
27. Suo Z, Wang W, Yang M (1994) Electromigration instability: transgranular slits in interconnects. *Appl Phys Lett* 64:1944
28. Yang W, Wang W, Suo Z (1994) Cavity and dislocation instability due to electric current. *J Mech Phys Solids* 42:897
29. Itô KE (1980) Methods other than difference methods. In: Iyanaga S, Kuwada Y (eds) *Encyclopedic dictionary of mathematics*, vol 2. MIT Press, Cambridge
30. Atkinson RR (2003) PhD, Rutgers, Multiphysics of degradation and failure of line interconnects. The State University of New Jersey, New Brunswick
31. Gungor MR, Maroudas D (1998) Electromigration-induced failure of metallic thin films due to transgranular void propagation. *Appl Phys Lett* 72:3452
32. Gungor MR, Maroudas D (1999) Theoretical analysis of electromigration-induced failure of metallic thin films due to transgranular void propagation. *J Appl Phys* 85:2233
33. Schimschak M, Krug J (2000) Electromigration-driven shape evolution of two-dimensional voids. *J Appl Phys* 87:695
34. Karma A, Rappel W (1996) Phase-field method for computationally efficient modeling of solidification with arbitrary interface kinetics. *Phys Rev E* 53:R3017
35. Mahadevan M, Bradley RM (1999) Simulations and theory of electromigration-induced slit formation in unpassivated single-crystal metal lines. *Phys Rev B* 59:11037
36. Mahadevan M, Bradley RM (1999) Simulations and theory of electromigration-induced slit formation in unpassivated single-crystal-metal lines. *Phys Rev B* 59:11037
37. Fix G (1983) Free boundary problems. In: Fasano A, Primicerio M (eds) *Research notes in mathematics*, vol 2. Pitman, New York

38. Collins JB, Levine H (1985) Diffuse interface model of diffusion-limited crystal growth. *Phys Rev B* 31:6119
39. Bhate DN, Kumar A, Bower AF (2000) Diffuse interface model for electromigration and stress voiding. *J Appl Phys* 87:1712
40. Gurtin M (1996) Generalized Ginzburg-Landau and Cahn-Hilliard equations based on a microforce balance. *Physica D* 92:178
41. Sauter Mack A, Flinn P (1995) Effect of intrinsic passivation stress on stress in encapsulated interconnect lines. In: *Materials Research Society Symposium*, Boston, MA, USA, pp 465–470
42. Yeo I-S, Ho PS (1996) Stress relaxation and microstructural change in passivated Al(Cu) lines. In: *34th Annual proceedings of reliability physics symposium*, Dallas, pp 131–138
43. Young-Chang J, Jong-Min P, Il-Mok P (2006) Effect of grain growth stress and stress gradient on stress-induced voiding in damascene Cu/low- k interconnects for ULSI. *Thin Solid Films* 504:284–287
44. Li C-Y, Borgesen P, Sullivan TD (1991) Stress-migration related electromigration damage mechanism in passivated, narrow interconnects. *Appl Phys Lett* 59:1464
45. Ogawa ET, Mcpherson JW, Rosal JA (2002) Stress-induced voiding under vias connected to wide Cu metal leads. In: *Proceedings of 40th Annual IEEE international reliability physics symposium (IRPS)*, pp 312–321
46. Wang TC, Hsieh TE, Wang M-T, Su D-S, Chang C-H, Wang YL, Lee JY-M (2005) Stress migration and electromigration improvement for copper dual damascene interconnection. *J Electrochem Soc* 152:45–49
47. Hommel M, Fischer AH, Glasow AV, Zitzelsberger AE (2002) Stress-induced voiding in aluminum and copper interconnects. In: *Stress-induced phenomena in metallization: Sixth international workshop on stress-induced phenomena in metallization*, pp 157–168
48. An JH, Ferreira PJ (2006) In situ transmission electron microscopy observations of 1.8 μm and 180 nm Cu interconnects under thermal stresses. *Appl Phys Lett* 89:151919
49. Fayolle M, Passemard G, Assous M, Louis D, Beverina A, Gobil Y, Cluzel J, Arnaud L (2002) Integration of copper with an organic low- k dielectric in 0.12 μm node interconnect. *Microelectron Eng* 60(1–2):119–124
50. Laconte J, Iker F, Jorez S, Andre N, Proost J, Pardoën T, Flandre D, Raskin JP (2004) Thin films stress extraction using micromachined structures and wafer curvature measurements. *Microelectron Eng* 76(1–2):219–226
51. Rivero C, Gergaud P, Gailhanou M, Thomas O, Froment B, Jaouen H, Carron V (2005) Combined synchrotron x-ray diffraction and wafer curvature measurements during Ni-Si reactive film formation. *Appl Phys Lett* 87:1–3
52. Budiman AS, Nix WD, Tamura N, Valek BC, Gadre K, Maiz J, Spolenak R, Patel JR (2006) Crystal plasticity in Cu damascene interconnect lines undergoing electromigration as revealed by synchrotron x-ray microdiffraction. *Appl Phys Lett* 88:233515
53. Rhee SH, Du Y, Ho PS (2003) Thermal stress characteristics of Cu/oxide and Cu/low- k submicron interconnect structures. *J Appl Phys* 93:3926–3933
54. Igic PM, Mawby PA (1999) An advanced finite element strategy for thermal stress field investigation in aluminium interconnections during processing of very large scale integration multilevel structures. *Microelectron J* 30:1207–1212
55. Shen Y-L (2006) Thermo-mechanical stresses in copper interconnects: a modeling analysis. *Microelectron Eng* 83:446–459
56. Paik J-M, Park H, Joo Y-C (2004) Effect of low- k dielectric on stress and stress-induced damage in Cu interconnects. *Microelectron Eng* 71:348–357
57. Flinn PA (1995) Mechanical stress in VLSI interconnections: origins, effects, measurement, and modeling. *Mater Res Bull* 20:70–73
58. Shi LT, Tu KN (1994) Finite-element modeling of stress distribution and migration in interconnecting studs of a three-dimensional multilevel device structure. *Appl Phys Lett* 65:1516

59. Ho PS, Yeo IS, Liao CN, Anderson SGH, Kawasaki H (1995) Thermal stress and relaxation behaviour of Al(Cu) submicroninterconnects. In: 4th International conference on solid-state and integrated circuit technology, Beijing, China, pp 408–412
60. Niwa H, Yagi H, Tsuchikawa H, Masaharu K (1990) Stress distribution in an aluminum interconnect of very large scale integration. *J Appl Phys* 68:328–333
61. Valek BC, Bravman JC, Tamura N, MacDowell AA, Celestre RS, Padmore HA, Spolenak R, Brown WL, Batterman BW, Patel JR (2002) Electromigration-induced plastic deformation in passivated metal lines. *Appl Phys Lett* 81:4168
62. Hou Y, Tan CM (2007) Blech effect in Cu interconencts with oxide and low-*k* dielectrics. In: 14th International symposium on the physics and failure analysis of integrated circuits, IEEE, Bangalore, India, p 65
63. Paik J-M, Park H, Joo Y-C, Park K-C (2005) Effect of dielectric materials on stress-induced damage modes in damascene Cu lines. *J Appl Phys* 97:104513
64. Korhonen MA, Black RD, Li C-Y (1991) Stress relaxation of passivated aluminum line metallizations on silicon substrates. *J Appl Phys* 69:1748–1755
65. Wikstrom A, Gudmundson P, Suresh S (1999) Analysis of average thermal stresses in passivated metal interconnects. *J Appl Phys* 86:6088–6095
66. Chang CW, Thompson CV, Gan CL, Pey KL, Choi WK, Lim YK (2007) Effects of microvoids on the linewidth dependence of electromigration failure of dual-damascene copper interconnects. *Appl Phys Lett* 90:193505
67. Shen Y-L, Guo YL, Minor CA (2000) Voiding induced stress redistribution and its reliability implications in metal interconnects. *Acta Mater* 48:1667–1678
68. Thouless MD, Rodbell KP, Cabral C (1996) Effect of a surface layer on the stress relaxation of thin films. *J Vacuum Sci Technol A* 14:2454
69. Keller R-M, Baker SP, Arzt E (1998) Quantitative analysis of strengthening mechanisms in thin Cu films: effects of film thickness, grain size and passivation. *J Mater Res* 13:1307–1317
70. Suo Z (2003) Reliability of interconnect structures. In: Gerberich W, Yang W (eds) *Comprehensive structural integrity*, vol 8. Elsevier, Amsterdam, pp 265–324
71. Hou Y, Tan CM (2008) Stress-induced voiding study in integrated circuit interconnects. *Semicond Sci Technol* 23:075023–075031
72. Korhonen MA, Black RD, Li C-Y (1993) Stress evolution due to electromigration in confined metal lines. *J Appl Phys* 73:3790–3799
73. Zhai CJ, Blish RC (2005) A physically based lifetime model for stress-induced voiding in interconnects. *J Appl Phys* 97:113503
74. Fischer AH, Zitzelsberger AE (2001) The quantitative assessment of stress-induced voiding in process qualification. In: *Proceedings of 39th IEEE/IRPS conference*, Orlando, Florida, IEEE, New York, pp 334–340
75. Tan CM, Hou Y (2007) Lifetime modeling for stress-induced voiding in integrated circuit interconnections. *Appl Phys Lett* 91:061904
76. Ogawa ET, McPherson JW, Rosal JA, Dickerson KJ, Chiu T-C, Tsung LY, Jain MK, Bonifield TD, Ondrusek JC, Mckee WR (2002) Stress-induced voiding under vias connected to wide Cu metal leads. In: *Proceedings of 40th IEEE/IRPS conference*, Dallas, Texas, IEEE, New York, pp 312–331
77. Aoyagi M, Asada K (1999) Vacancy distribution in aluminum interconnections on semiconductor devices. *Jpn J Appl Phys* 38:1909–1914 Part 1 (Regular Papers, Short Notes & Review Papers)
78. Aoyagi M (2003) Modeling of vacancy flux due to stress-induced migration. *J Vacuum Sci Technol B Microelectron Nanometer Struct* 21:1314–1317
79. Aoyagi M (2006) Change in electrical resistance caused by stress-induced migration. *J Vacuum Sci Technol B Microelectron Nanometer Struct* 24:250–254
80. Reimbold G, Sicardy O, Arnaud L, Fillot F, Torres J (2002) Mechanical stress measurements in damascene copper interconnects and influence on electromigration parameters. *IEDM Tech Digest* 745–748

81. Bruynseraede C, Tokei Z, Iacopi F, Beyer GP, Michelon J, Maex K (2005) The impact of scaling on electromigration reliability. In: Proceedings of 43rd IEEE/IRPS conference, pp 7–17
82. Suo Z (2003) Interfacial and Nanoscale Failure. In: Gerberich W, Yang W (eds) Reliability of interconnect structures. Comprehensive Structural Integrity (Milne I, Ritchie RO, Karihaloo B, Editors-in-Chief), 8:265–324
83. Gan ZH, Shao W, Mhaisalkar SG, Chen Z, Gusak A (2006) Experimental and numerical studies of stress migration in Cu interconnects embedded in different dielectrics. In: Stress-induced phenomena in metallization. Eighth international workshop on stress-induced phenomena in metallization, AIP, vol 817, pp 269–274
84. Hau-Riege CS, Hau-Riege SP, Marathe AP (2004) The effect of interlevel dielectric on the critical tensile stress to void nucleation for the reliability of Cu interconnects. *J Appl Phys* 96:5792–5796
85. Tan CM, Hou Y, Li W (2007) Revisit to the finite element modeling of electromigration for narrow interconnects. *J Appl Phys* 102:033705
86. Sharma P, Ganti S, Ardebili H, Alizadeh A (2004) On the scaling of thermal stresses in passivated nanointerconnects. *J Appl Phys* 95:2763–2769
87. Chiras S, Charke DR (2000) Dielectric cracking produced by electromigration in microelectronic interconnects. *J Appl Phys* 88:6302–6312
88. Atrash F, Sherman D (2006) Analysis of the residual stresses, the biaxial modulus, and the interfacial fracture energy of low- k dielectric thin films. *J Appl Phys* 100:103510–103517
89. Du Y, Wang G, Merrill C, Ho PS (2002) Thermal stress and debonding in Cu/low- k damascene line structures. In: 52nd Electronic components and technology conference, pp 859–864
90. Shen Y-L, Ramamurty U (2003) Temperature-dependent inelastic response of passivated copper films: experiments, analyses, and implications. *J Vacuum Sci Technol B* 21:1258–1264

Applications of Finite Element Methods for Reliability
Studies on ULSI Interconnections

Tan, C.M.; Li, W.; Gan, Z.; Hou, Y.

2011, VIII, 152 p., Hardcover

ISBN: 978-0-85729-309-1